A Parameterization Scheme for Lossy Transmission Line Macromodels with Application to High Speed Interconnects in Mobile Devices

A Parameterization Scheme for Lossy Transmission Line Macromodels With Application to High Speed Interconnects in Mobile Devices

Stefano Grivet-Talocia, *Member, IEEE*, Silvia Acquadro, Michelangelo Bandinu, Flavio G. Canavero, *Fellow, IEEE*, Ilkka Kelander, and Makku Rouvala

***Abstract*—We introduce a novel parameterization scheme based on the generalized method of characteristics (MoC) for macromodels of transmission-line structures having a cross section depending on several free geometrical and material parameters. This situation is common in early design stages, when the physical structures still have to be finalized and optimized under signal integrity and electromagnetic compatibility constraints. The topology of the adopted line macromodels has been demonstrated to guarantee excellent accuracy and efficiency. The key factors are propagation delay extraction and rational approximations, which intrinsically lead to a SPICE-compatible macromodel stamp. We introduce a scheme that parameterizes this stamp as a function of geometrical and material parameters such as conductor-width and separation, dielectric thickness, and permettivity. The parameterization is performed via multidimensional interpolation of the residue matrices in the rational approximation of characteristic admittance and propagation operators. A significant advantage of this approach consists of the possibility of efficiently utilizing the MoC methodology in an optimization scheme and eventually helping the design of interconnects. We apply the proposed scheme to flexible printed interconnects that are typically found in portable devices having moving parts. Several validations demonstrate the effectiveness of the approach.**

***Index Terms*—Interpolation, parametric modeling, rational approximation, transmission line modeling.**

I. Introduction

SIGNAL degradation in electrical interconnects is one of the major limiting factors in the performance of high-speed electronic systems. In fact, when the data bandwidth transferred through the interconnect is increased and miniaturization is nearly pushed to manufacturing capabilities, the electrical properties become increasingly more important in order to maintain good signal quality. Once the interconnect technology is chosen, some form of optimization is required in very early stages of the physical design in order to select the cross-sectional configuration of the interconnect providing the best electrical performance. At this stage, the entire cross section is still undefined, with all relevant geometrical parameters (conductor width, height, separation, and dielectric height) and material parameters (dielectric permettivity and metal conductivity) being specified via ranges of variation rather than fixed values. Suitable tools must be available to the designer to guide his choices, since the number of free parameters may be quite large, and a full electromagnetic analysis covering the entire parameter space is obviously unfeasible.

In this paper, we introduce a parameterization scheme aimed at the reduction of the computational burden that would be required by extensive electromagnetic simulation. In particular, we consider a generic lossy and frequency-dependent multiconductor transmission line segment, and we cast its terminal port equations in the form of the generalized method of characteristics (MoC) [1], [2]. Basic components of this formulation are asymptotic modal delay extraction and low-order rational approximations of characteristic admittance and delayless propagation operators. This representation describes the interconnect as a multiport governed by delayed ordinary differential equations, which can be easily synthesized into a SPICE-compatible equivalent circuit using only standard elements. The main new contribution of this paper is the parameterization of this equivalent circuit as a function of a varying cross-sectional geometry of the transmission line. This is obtained by applying smooth interpolation schemes to the residue matrices of the above-mentioned rational approximations. Other complementary approaches for parameterized macromodeling of transmission line in the framework of model order reduction are available in [3] and [4].

Although the parameterization scheme presented in this paper is general and, in principle, applicable to any transmission line structure, all numerical examples will be targeted to interconnects for mobile devices. In particular, we focus on flexible interconnects going through hinges in foldable mobile phones and connecting electrical modules residing in different moving blocks. An example can be the connection between a display module, typically in the upper block of the device, and a computing module, which usually is in the lower block. Such interconnections are commonly realized using flexible printed circuits (FPC) in order to guarantee good flexibility and bendability. For this particular application, we show that the proposed macromodeling strategy requires a limited number of field solutions for the computation of the per-unit-length matrices over a very coarse discrete grid in the parameter space. However, the parameterized macromodels are able to represent, with excellent accuracy, the continuous dependence of the transmission line electrical behavior on each of the considered parameters.

Manuscript received February 23, 2006; revised October 5, 2006.

S. Grivet-Talocia, S. Acquadro, M. Bandinu, and F. G. Canavero are with Politecnico di Torino, I-10129 Turin, Italy (e-mail: grivet@polito.it; silvia.acquadro@delen.polito.it; bandinu@delen.polito.it; flavio.canavero@polito.it).

I. Kelander and M. Rouvala are with Nokia Research Center, FIN-00180 Helsinki, Finland (e-mail: ilkka.kelander@nokia.com; markku.rouvala@nokia.com).

Digital Object Identifier 10.1109/TEMC.2007.888179

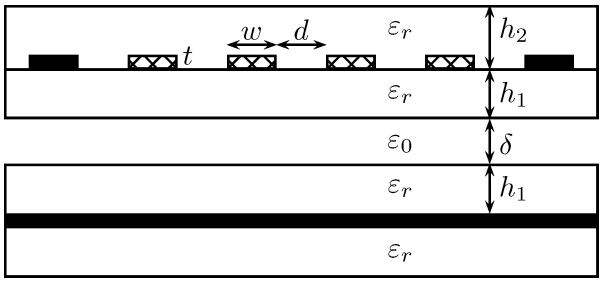

Fig. 1. Cross section of the (type B) transmission line under investigation with the defintion of relevant geometrical/material parameters. Type A is without bottom ground layer and type C has an additional (identical) top ground layer. *Crosshatch* and *solid fill* indicate signal and ground conductors, respectively.

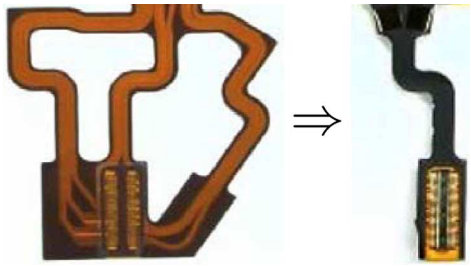

Fig. 2. "Origami style" multilayer FPC (single layer FPC is folded twice).

We first introduce the structures under investigation in Section II. The complete macromodeling process and its parameterization are presented and discussed in Section III. Finally, numerical results and validations on several test cases are presented in Section IV.

II. Flexible Interconnects for Mobile Devices

The cross section of a typical FPC interconnect is depicted in Fig. 1. Flexible printed interconnects can be considered as planar layered structures, with usually more than one conductor layer. Each single layer has the conducting part buried between top and bottom dielectric covers. One possibility to obtain multiple layers is to stack single-layer FPCs, as shown in Fig. 2. This may induce the presence of an airgap δ between the different layers, as depicted in Fig. 1.

We consider here three different classes of FPC interconnects with one signal layer, depicted in Fig. 1. The three structures differ only for the presence of a bottom and top ground (return) layers and are labeled type A (no ground layers), type B (only bottom ground layer), and type C (top and bottom ground layers). The signal layer includes four actual signal lines and two lateral ground lines. The geometrical parameters (conductor width w and separation d, dielectric thickness h, etc.) and electrical parameters (dielectric constant ε_r) are specified as ranges of variation and are summarized in Table I. All these parameters will be collected in a m-dimensional array $\lambda = (\lambda_1, \ldots, \lambda_m)$, excluding the line length $\mathcal{L}$, which will be treated differently from the other parameters.

TABLE I
Geometrical and Material Line Parameters

Parameter	Min	Max
h_1	50 μm	50 μm
h_2	50 μm	65 μm
δ	0 mm	1 mm
w	50 μm	150 μm
d	w	$2w$
t	17.5 μm	17.5 μm
ε_r	3.2	4.0
Length	0 mm	300 mm

We describe the interconnect as a uniform transmission line governed by parameterized telegraphers' equations

$$-\frac{d}{dz}\mathbf{V}(z,s;\lambda) = [\mathbf{R}(s;\lambda) + s\mathbf{L}(s;\lambda)]\,\mathbf{I}(z,s;\lambda)$$
$$-\frac{d}{dz}\mathbf{I}(z,s;\lambda) = [\mathbf{G}(s;\lambda) + s\mathbf{C}(s;\lambda)]\,\mathbf{V}(z,s;\lambda) \quad (1)$$

where s is the Laplace variable, and $\mathbf{G}(s;\lambda), \mathbf{C}(s;\lambda), \mathbf{R}(s;\lambda)$, and $\mathbf{L}(s;\lambda)$ denote the frequency-dependent parameterized per-unit-length conductance, capacitance, resistance, and inductance matrices, respectively. In this paper, we neglect dielectric losses; therefore, the conductance matrices are vanishing, and the per-unit-length capacitance matrices are constant throughout frequency

$$\mathbf{G}(s;\lambda) = \mathbf{0}, \quad \mathbf{C}(s;\lambda) = \mathbf{C}(\lambda). \quad (2)$$

We remark that dielectric losses may be significant for present application due to the broadband nature of the signals that are intended to propagate along the interconnect. However, we are missing at the moment a reliable set of broadband data for the loss tangent of the dielectric material. Future investigations will also include such information. Note that the model derivation and parameterization technique is valid for an arbitrary frequency dependence of all per-unit-length matrices.

The computation of the capacitance matrix is performed by application of the method-of-moments (MoM) techinque of [5]. Instead, the full frequency dependence of line resistance and inductance are considered in order to include skin-effect losses. The two-dimensional (2-D) quasi-magnetostatic Green's function of the planar structure is approximated via the procedure outlined in [6]. Then, the current density in the conductors is discretized using an adaptive and frequency-dependent mesh. A standard 2-D MoM formulation allows us to compute the per-unit-length resistance and inductance matrices over a broad frequency range from dc up to 10 GHz.

The above computations can be performed for a single combination of the m parameters controlling the cross-sectional geometry. However, in order to recover a complete characterization and dependence on each of the m individual parameters, the same computations have to be repeated on a sufficiently accurate grid $\{\lambda^{(\nu)},\ \nu = 1, \ldots, p\}$ of points in the parameter space. In order to reduce the computational cost of this characterization, it is important to minimize the number of grid points. We will show that a quite coarse grid combined with suitable interpolation schemes is sufficient for our purposes.

III. Line Parameterization and Macromodeling

The macromodeling procedure follows from [2], extending all derivations to the parameterized case. The transmission line segment is treated as a multiport, with $\mathbf{V}_1, \mathbf{I}_1$ and $\mathbf{V}_2, \mathbf{I}_2$ denoting the near and far-end terminal voltage and current vectors. In the framework of the MoC, the solution of (1) can be restated as

$$\begin{aligned}\mathbf{I}_1 &= \mathbf{Y}_c(s;\lambda)\mathbf{V}_1 - \mathbf{H}(s;\lambda)\left[\mathbf{Y}_c(s;\lambda)\mathbf{V}_2 + \mathbf{I}_2\right]\\ \mathbf{I}_2 &= \mathbf{Y}_c(s;\lambda)\mathbf{V}_2 - \mathbf{H}(s;\lambda)\left[\mathbf{Y}_c(s;\lambda)\mathbf{V}_1 + \mathbf{I}_1\right]\end{aligned} \tag{3}$$

with

$$\begin{aligned}\mathbf{\Gamma}^2(s;\lambda) &= [\mathbf{G}(s;\lambda) + s\mathbf{C}(s;\lambda)][\mathbf{R}(s;\lambda) + s\mathbf{L}(s;\lambda)]\\ \mathbf{Y}_c(s;\lambda) &= \mathbf{\Gamma}^{-1}(s;\lambda)[\mathbf{G}(s;\lambda) + s\mathbf{C}(s;\lambda)]\\ \mathbf{H}(s;\lambda) &= e^{-\mathcal{L}\mathbf{\Gamma}(s;\lambda)}\end{aligned} \tag{4}$$

being the squared propagation matrix, the characteristic admittance matrix, and the propagation operator matrix for a line length $\mathcal{L}$, respectively.

The key point enabling the construction of a macromodel suitable for time-domain analysis will be the approximation of $\mathbf{Y}_c(s;\lambda)$ and $\mathbf{H}(s;\lambda)$ as a combination of rational functions of frequency and pure delay terms. In fact, this approximation leads naturally to a system of delayed ordinary differential equations and allows the macromodel to be synthesized into an equivalent circuit using only standard elements. A complete description is found in [2]. The main difficulty with which we deal in this paper is the parameterization of such delayed rational approximations.

A. Delay Extraction

One possibility for delay extraction is provided by asymptotic modal decomposition. Considering the high-frequency ($s \to \infty$) capacitance and inductance matrices, the eigendecomposition is

$$\mathbf{\Lambda}(\lambda) = \mathbf{M}^{-1}(\lambda)\,\mathbf{C}(\infty;\lambda)\,\mathbf{L}(\infty;\lambda)\,\mathbf{M}(\lambda) \tag{5}$$

where $\mathbf{M}(\lambda)$ collects the high-frequency modal profiles, and $\mathbf{\Lambda}(\lambda)$ is diagonal. The high-frequency modal delays are then defined as

$$T_k(\lambda) = \mathcal{L}\sqrt{\Lambda_{kk}(\lambda)} \tag{6}$$

for a line length $\mathcal{L}$. Once these delays are computed, modal delay extraction can be performed via

$$\mathbf{P}(s;\lambda) = \mathrm{diag}\{e^{sT_k(\lambda)}\}\,\mathbf{M}^{-1}(\lambda)\,\mathbf{H}(s;\lambda)\,\mathbf{M}(\lambda). \tag{7}$$

The above matrix operator mainly represents line attenuation and dispersion for each asymptotic modal profile, whereas the finite propagation delay is explicitly represented by the pure exponential terms. The effectiveness of this approach is evident in Fig. 3, where $\mathbf{H}(s;\lambda)$ and $\mathbf{P}(s;\lambda)$ are compared for two different line lengths. It should be noted that the model complexity depends on the line length if no delay extraction is performed, while the delayless operator $\mathbf{P}(s;\lambda)$ exploits almost no dependence on line length.

The above strategy, which is the core of the Topline methodology [2], was used in [7], where a simple two-conductor line

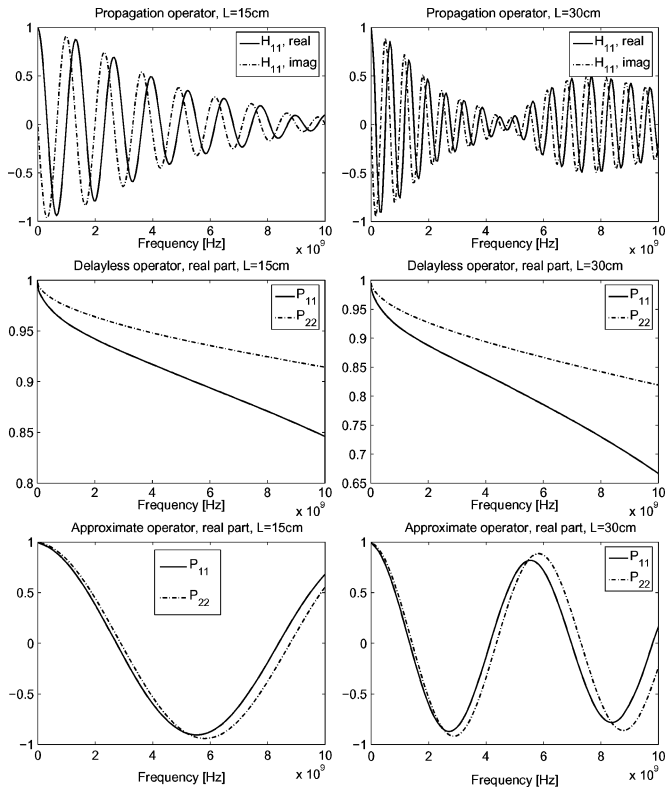

Fig. 3. (Top) Propagation operator $\mathbf{H}(s;\lambda)$ for type B structure and two different line lengths $\mathcal{L} = 15$ cm (left) and $\mathcal{L} = 30$ cm (right). (Middle) Delayless modal propagation operator $\mathbf{P}(s;\lambda)$ with full delay extraction. (Bottom) Approximate delayless modal propagation operator $\tilde{\mathbf{P}}(s;\lambda)$ with partial delay extraction.

was analyzed. In the results of [7], only a weak parameter-dependence of the modal delays was observed. Also, due to symmetry consideration, the asymptotic modes were equivalent to the standard even/odd modal profiles, which in turn provided a diagonalization of the transmission line equations at all frequencies and uniformly over the entire parameter space. These assumptions do not hold for the more general case that is investigated here. Full diagonalization is dependent on frequency, and the modal profiles are highly dependent on the geometrical parameters λ. Therefore, we are faced with the alternative of

1) preserving accuracy as much as possible, by retaining the parameter-dependence of both modal profiles and modal delays, as in (7);
2) releasing slightly the accuracy constraints, by forcing constant "modes" throughout the parameter space.

After extensive testing, we decided to follow the second strategy. Indeed, taking into account the full parameter- and possibly frequency-dependence of the modes leads to inherent difficulties due to their possibly large sensitivities. We will show that quite significant simplifications involved in the second strategy have only a negligible impact on the accuracy of the macromodel.

B. Approximate Delay Extraction

The proposed delay extraction scheme is as follows. We define an approximate "modal" transformation matrix as

$$\bar{\mathbf{M}} = \mathbf{M}(\bar{\lambda}) \tag{8}$$

where $\bar{\lambda}$ denotes a specific point in the parameter space. In order to maximize accuracy, we use the mean value for each component as

$$\bar{\lambda}_i = \frac{\lambda_{i,\max} + \lambda_{i,\min}}{2} \tag{9}$$

taking the upper and lower bounds as in Table I. Note that the columns of matrix $\bar{\mathbf{M}}$ represent asymptotic modes only for $\lambda = \bar{\lambda}$. For different parameter combinations, they only provide approximations of the asymptotic modal profiles. Nonetheless, we will denote $\bar{\mathbf{M}}$ as a "modal" matrix with a slight abuse of notation. Then, we compute

$$\bar{\mathbf{\Lambda}}(\lambda) = \bar{\mathbf{M}}^{-1}\,\mathbf{C}(\infty;\lambda)\,\mathbf{L}(\infty;\lambda)\,\bar{\mathbf{M}}. \tag{10}$$

This matrix is not diagonal since the modes are not exact, but it can be viewed as a small perturbation of the diagonal matrix defined in (5). The (squared) amount of this perturbation is estimated as

$$\alpha^2 = \max_{\lambda} \frac{\|\bar{\mathbf{\Lambda}}(\lambda) - \mathbf{\Lambda}(\lambda)\|}{\|\mathbf{\Lambda}(\lambda)\|}. \tag{11}$$

We now define a set of approximate parameter-dependent modal delays as

$$\tilde{T}_k(\lambda) = (1-\alpha)\mathcal{L}\sqrt{\bar{\Lambda}_{kk}(\lambda)}. \tag{12}$$

A few comments about this definition are in order. First, these delays are exact for the mean parameter configuration $\lambda = \bar{\lambda}$, in which case, $\tilde{T}_k(\lambda) = T_k(\lambda)$ when $\alpha = 0$. Second, the delays in (12) are allowed to be slightly less than the exact delays computed via (6), since $\alpha > 0$, but the difference is small when the approximate modes in $\bar{\mathbf{M}}$ are close to the actual modes $\mathbf{M}(\lambda)$. Third, the delays in (12) can be viewed as first-order approximations of the exact delays as

$$\tilde{T}_k(\lambda) = T_k(\lambda) + \Delta T_k(\lambda). \tag{13}$$

The $(1-\alpha)$ factor ensures that the sign of the perturbation term $\Delta T_k(\lambda)$ is negative, so that each $\tilde{T}_k(\lambda)$ is not larger than the corresponding physics-based modal delay $T_k(\lambda)$. If this condition were violated, noncausal behaviors might be obtained due to the delay extraction procedure, which is defined next. Fourth, (12) preserves the relative difference between each pair of approximate modal delays. It is clear that the entire procedure is valid only when $\alpha \ll 1$, which allows us to keep the accuracy under control. In all tests that we performed, we detected maximum perturbation amounts $\alpha \leq 0.1$, thus enabling and validating the approximate formulation.

An approximate delayless modal propagation operator is now defined as

$$\tilde{\mathbf{P}}(s;\lambda) = \mathrm{diag}\{e^{s\tilde{T}_k(\lambda)}\}\bar{\mathbf{M}}^{-1}\mathbf{H}(s;\lambda)\bar{\mathbf{M}}. \tag{14}$$

The bottom panels in Fig. 3 show the frequency behavior of this operator. As expected, a residual delay is clearly visible for $\tilde{\mathbf{P}}(s;\lambda)$, with a limited length dependence. However, a comparison with $\mathbf{H}(s;\lambda)$ (top panels in the figure) demonstrates that most of the delay has been extracted. The main advantage of (14) with respect to (7) is due to the approximate modes that do not depend on λ and which, therefore, do not need any parameterization.

C. Rational Approximations

Once the delay terms have been extracted, rational approximations of $\mathbf{Y}_c(s;\lambda)$ and $\tilde{\mathbf{P}}(s;\lambda)$ are computed. The feasibility of such rational approximations is confirmed by the smooth frequency behavior of both matrix operators. During this phase, a suitable interpolation scheme must also be devised for the representation of such approximations over the entire parameter space, given the finite number p of samples that are actually available. After extensive testing, we adopted the representation

$$\mathbf{Y}_c(s;\lambda) \simeq \sum_n \frac{\mathbf{R}_n^Y(\lambda)}{s-p_n} + \mathbf{Y}_\infty(\lambda)$$

$$\tilde{\mathbf{P}}(s;\lambda) \simeq \sum_n \frac{\mathbf{R}_n^P(\lambda)}{s-q_n} + \mathbf{P}_\infty(\lambda) \tag{15}$$

characterized by common poles throughout the parameter space and by parameter-dependent residues and direct couplings. The computation of the poles is performed by applying the well-known vector fitting (VF) algorithm [8]. In order to maximize accuracy, the entire set of p realizations is included in a single VF run. This is possible since the number of frequency samples is quite small (around 40 from almost dc to 10 GHz) with logarithmic spacing. Residues and direct coupling matrices in (15) are then computed via separate linear least squares problems for each of the p parameter combinations. Finally, a continuous variation throughout the parameter space is recovered as

$$\mathbf{R}_n^Y(\lambda) = \sum_\nu \theta_n^\nu \mathbf{R}_n^Y(\lambda^{(\nu)}) \tag{16}$$

and similarly for the other parameter-dependent matrices in (15) and for the delays $\tilde{T}_k(\lambda)$. The coefficients θ_n^ν are determined by multidimensional interpolation. The actual choice of this interpolation scheme is very important and is the subject of the following section. We remark that there is no need for parameterization of the modal matrix since it is assumed to be constant throughout the parameter space.

D. Parameterization Schemes

The variations induced by each individual parameter were investigated by computing the per-unit-length matrices on a sufficiently fine grid of points in the parameter space. Then, we derived $\mathbf{Y}_c(s;\lambda)$, $\tilde{\mathbf{P}}(s;\lambda)$, and the set of approximate modal delays $\tilde{T}_k(\lambda)$. We report in Fig. 4 the behavior of the characteristic admittance only since similar conclusions could be drawn by considering the other quantities.

The various parameters under consideration can be divided into four classes. First, the dielectric cover height h_2 and the dielectric constant ε_r induce only quasi-linear variations (top row in Fig. 4). Standard linear interpolation was then chosen to represent these parameters in (16). Second, the conductor width w and separation d were observed to induce very smooth and slow variations but with a sufficient deviation from linearity that would make a pure linear interpolation not sufficiently accurate (middle row in Fig. 4). Cubic spline interpolation was considered

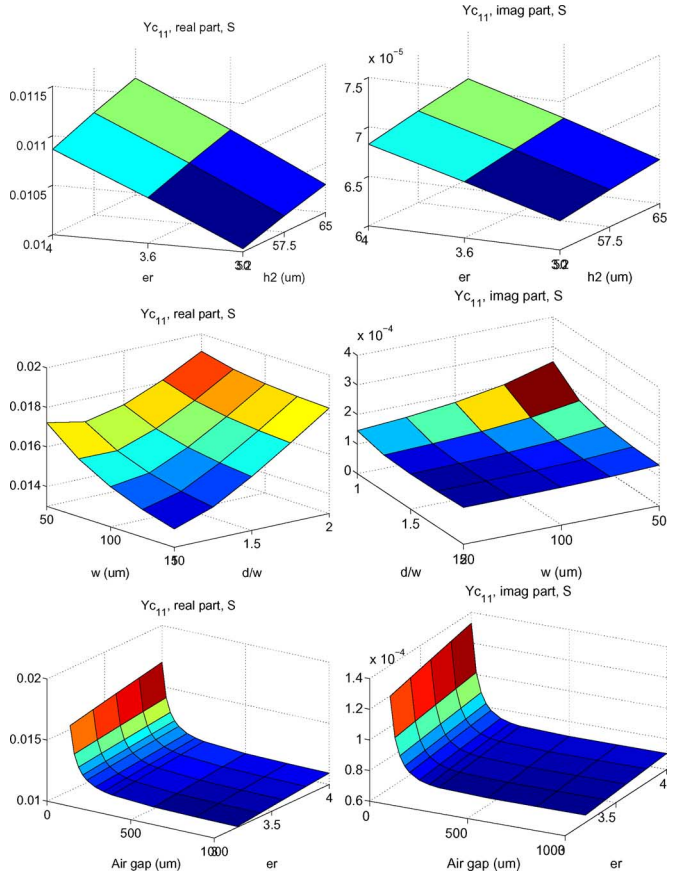

Fig. 4. Parameter-induced variations on selected entries of the characteristic admittance. (Top) Quasi-linear variations (h_2 and ε_r). (Middle) Slow variations (w and d/w). (Bottom) Fast variations (air gap δ).

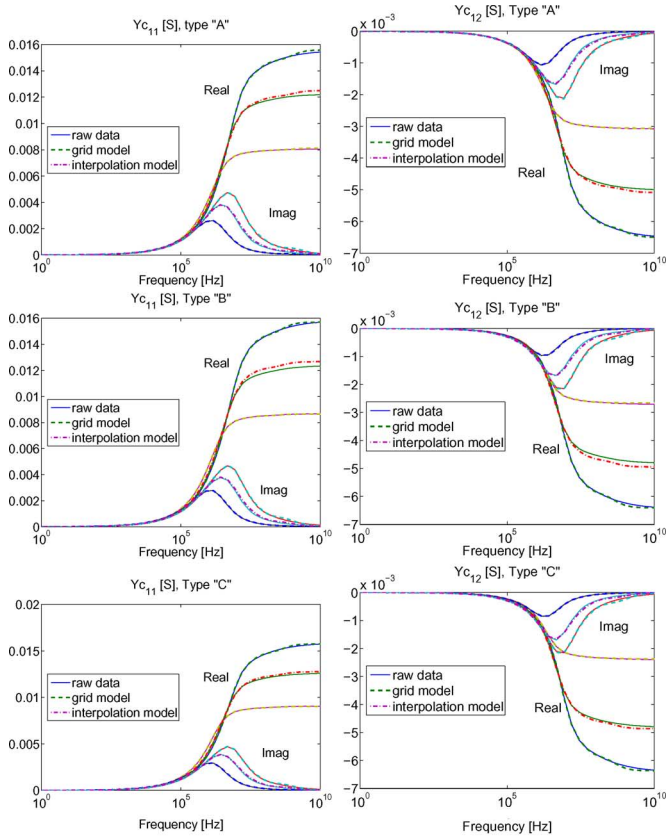

Fig. 5. Validation of the proposed interpolation scheme for two selected entries of the characteristic admittance $\mathbf{Y}_c(s;\lambda)$. In each panel, *upper* and *lower* sets of curves correspond to grid points $\lambda^{(k)}$ in the parameter space where raw data is available. Curves that are in *between* correspond to a validation point for the interpolated model.

for these two parameters. The approximate modal delays $\tilde{T}_k(\lambda)$ also fall into this class. Third, the airgap δ still induces smooth variations but with increased rate for small gap values (last row in Fig. 4). In this paper, we exclude the gap from the set of free parameters, although we verified that a single-pole rational interpolation/approximation gives excellent accuracy. In fact, an airgap is generated between two FPC layers when the layers are turned and slid over each other in moving mechanisms. This is due to length difference of the two layers in the turning point due to different radii of the layers. A sound model should include variability of the air gap along the propagation direction as $\delta = \delta(z)$, thus requiring a nonuniform trasmission line model. However, the extension of MoC-based macromodeling techniques to nonuniform lines is still an open problem. A simplistic approach might consider segmenting the line into small sections having constant parameters. This choice should be avoided since the main advantage of MoC schemes, i.e., high efficiency, would be completely lost. Since new theoretical developments are needed, this extension will be considered in future research. Finally, the line length is intrinsically and explicitly parameterized in (12) and does not need additional discussion.

IV. Numerical Result and Validation

We report here a few validations of the proposed parameterized macromodeling scheme for the three FPC types of Fig. 1. We start by reporting selected entries of the characteristic admittance in Fig. 5. These results correspond to fixed parameter values $\delta = 0.5$ mm, $\varepsilon_r = 3.6$, and $h_2 = 57.5\,\mu$m. The conductor width w and separation d/w were considered on a 3×3 grid (minimum, mean, and maximum value for each varying parameter) for the macromodel generation. Upper and lower sets of curves in each panel of Fig. 5 correspond to the two combinations with minimum and maximum values for both w and d/w. Finally, a validation point was selected with $w = 125\,\mu$m and $d/w = 1.75$. The corresponding macromodel was obtained via multidimensional interpolation. The raw frequency samples for validation were determined via (4) after a dedicated 2-D field solution, but these samples were not used for the generation of the macromodel. The intermediate curves in each panel of Fig. 5 report these validations. These plots show that 1) the accuracy of the rational approximation is excellent and 2) that the unavoidable errors introduced by the interpolation scheme are almost negligible.

We focus now on the approximate delayless operator $\tilde{\mathbf{P}}(s;\lambda)$. Fig. 6 reports the same set of validations already presented for the characteristic admittance in Fig. 5. We remark that these plots confirm the quite low sensitivity of the delayless propagation operator with respect to the cross-sectional geometry. This was expected since this operator mainly represents

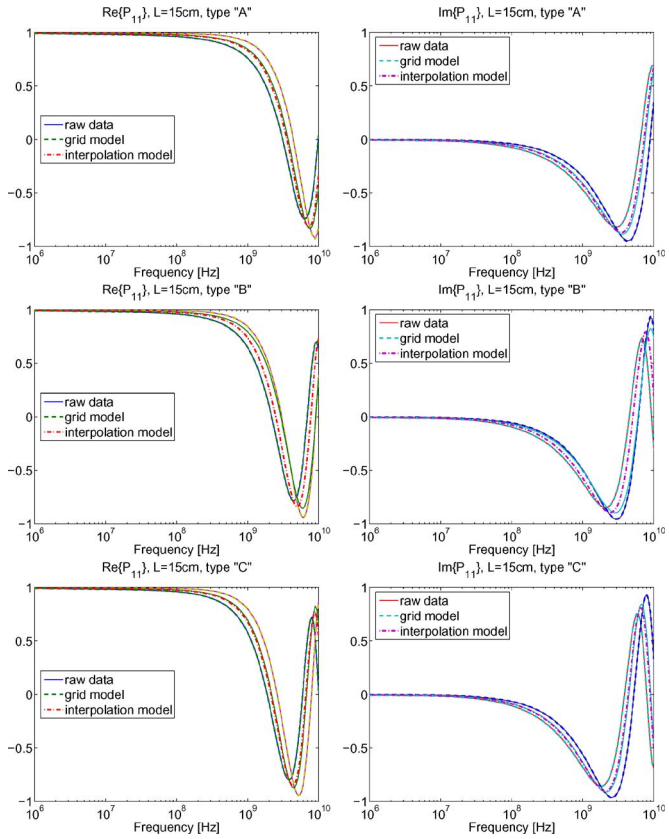

Fig. 6. Validation of the proposed interpolation scheme for a selected entry of the delayless propagation operator $\tilde{\mathbf{P}}(s;\lambda)$. As in Fig. 5, the *upper* and *lower* sets of curves in each panel correspond to grid points $\lambda^{(k)}$ in the parameter space where raw data is available. Curves that are in *between* correspond to a validation point for the interpolated model.

frequency-dependent attenuation and dispersion effects, which have a very weak dependence on the specific geometry configuration.

Finally, the true (delayed) propagation operator is recovered as

$$\mathbf{H}(s;\lambda) = \bar{\mathbf{M}}\,\mathrm{diag}\{e^{-s\tilde{T}_k(\lambda)}\}\,\tilde{\mathbf{P}}(s;\lambda)\,\bar{\mathbf{M}}^{-1}. \qquad (17)$$

Fig. 7 reports the frequency dependence of $\mathbf{H}(s;\lambda)$ for two different lengths of the type B FPC. Top panels correspond to a parameter configuration $\lambda^{(\nu)}$, which is available as a grid point. Therefore, no interpolation is involved in the generation of these curves, which provide a validation of the proposed combined delay extraction and rational approximation and demonstrate accuracy in the representation of the length-dependent standing-wave pattern. The bottom panels correspond to a parameter configuration λ, which is not available as a grid point (the same point already considered in Figs. 5 and 6), thus also including the interpolation effects. We remark that this final result is achieved with a macromodel complexity (number of poles), which is almost independent on the line length since the phase variations induced by the delay terms are treated independently.

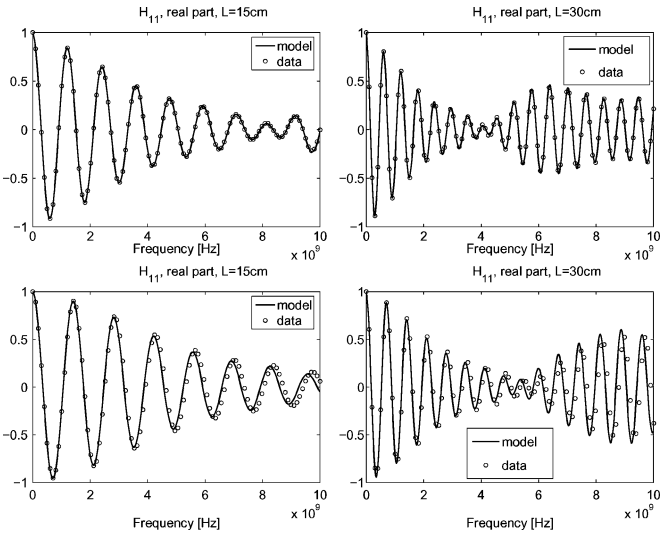

Fig. 7. Reconstructed propagation operator $\mathbf{H}(s;\lambda)$ for type B structure. (Top) Grid points in the parameter space where raw data is available. (Bottom) Validation point for the interpolated model.

V. Conclusion

We have presented a procedure for including the effects of varying electrical and geometrical parameters in macromodels of lossy transmission lines. A combination of delay extraction and rational approximations allows the casting of the macromodels in a form that is accepted by any standard circuit solver. On the other hand, the specific model representation, which is based on an extension of the well-known MoC, leads to a very smooth dependence on the relevant geometrical and electrical parameters of the structure, allowing for simple interpolation schemes to recover a continuous model dependence on the parameters. As a result, the model complexity is almost independent of the line length.

The proposed modeling scheme is applied to the representation of flexible printed interconnects present in modern cellular phones having moving parts. The resulting accuracy is excellent throughout the parameter space for all interconnects that were analyzed. The availability of accurate parameterized macromodels for such interconnects will allow systematic analysis of critical electrical links in the time domain with realistic (nonlinear/dynamic) driver and receiver networks. This, in turn, will allow link optimization under signal integrity constraints, with a consequent speedup in the overall interconnect design process. Preliminary results in this direction are available in [9].

References

[1] F. H. Branin, Jr., "Transient analysis of lossless transmission lines," *Proc. IEEE*, vol. 55, no. 11, pp. 2012–2013, Nov. 1967.

[2] S. Grivet-Talocia, H. M. Huang, A. E. Ruehli, F. Canavero, and I. M. Elfadel, "Transient analysis of lossy transmission lines: An effective approach based on the method of characteristics," *IEEE Trans. Adv. Packag.*, vol. 27, no. 1, pp. 45–56, Feb. 2004.

[3] P. Gunupudi, R. Khazaka, and M. Nakhla, "Analysis of transmission line circuits using multidimensional model reduction techniques," *IEEE Trans. Adv. Packag.*, vol. 25, no. 2, pp. 174–180, May 2002.

[4] P. K. Gunupudi, R. Khazaka, M. S. Nakhla, T. Smy, and D. Celo, "Passive parameterized time-domain macromodels for high-speed

transmission-line networks," *IEEE Trans. Microw. Theory Tech.*, vol. 51, no. 12, pp. 2347–2354, Dec. 2003.

[5] C. Wei, R. F. Harrington, J. R. Mautz, and T. Sarkar, "Multiconductor transmission lines in multilayered dielectric media," *IEEE Trans. Microw. Theory Tech.*, vol. MTT-32, no. 4, pp. 439–450, Apr. 1984.

[6] K. M. Coperich, J. Morsey, V. I. Okhmatovski, A. C. Cangellaris, and A. E. Ruehli, "Systematic development of transmission-line models for interconnects with frequency-dependent losses," *IEEE Trans. Microw. Theory Tech.*, vol. 49, no. 10, pp. 1677–1685, Oct. 2001.

[7] S. Grivet-Talocia, S. Acquadro, C. Peraldo, F. Canavero, I. Kelander, M. Rouvala, and A. Arslan, "Parameterized macromodels for lossy multiconductor transmission lines," in *Proc. 17th Int. Zurich Symp. Electromagn. Compat.*, Singapore, Feb. 27–Mar. 3, 2006, pp. 93–96.

[8] B. Gustavsen and A. Semlyen, "Rational approximation of frequency domain responses by vector fitting," *IEEE Trans. Power Del.*, vol. 14, no. 3, pp. 1052–1061, Jul. 1999.

[9] S. Grivet-Talocia, S. Acquadro, M. Bandinu, F. Canavero, I. Kelander, and M. Rouvala, "Signal integrity constrained optimization of flexible printed interconnects for mobile devices," in *Proc. IEEE Electromagn. Compat. Symp.,* vol. 3, Aug. 14–18, 2006, pp. 636–641.

Stefano Grivet-Talocia (M'98) received the Laurea and Ph.D. degrees in electronic engineering from the Politecnico di Torino, Turin, Italy.

From 1994 to 1996, he was at NASA/Goddard Space Flight Center, Greenbelt, MD, where he worked on applications of fractal geometry and wavelet transform to the analysis and processing of geophysical time series. He is currently an Associate Professor of circuit theory in the Department of Electronics, Politecnico di Torino. His current research interests include passive macromodeling of lumped and distributed interconnect structures, modeling and simulation of fields, circuits, and their interaction, wavelets, and time-frequency transforms and their applications. He is the author of more than 80 papers published in various journals and conference papers.

Dr. Grivet-Talocia was an Associate Editor for the IEEE TRANSACTIONS ON ELECTROMAGNETIC COMPATIBILITY.

Silvia Acquadro received the Laurea degree in electronic engineering from the Politecnico di Torino, Turin, Italy, in 2004.

Since 2004, she has been a Research Assistant with the EMC Group at the Politecnico di Torino. She has developed a computer code based on the method of moments for line parameter evaluation. Her current research interests include characterization of lossy and dispersive multiconductor interconnects via two- and three-dimensional modeling and parameterized macromodels of lumped and distributed interconnects.

Michelangelo Bandinu received the Laurea degree in electronic engineering from the Politecnico di Torino, Turin, Italy, in 2005.

He was with IBM Deutschland Entwicklung GmbH, Boeblingen, Germany, where he was working in the field of packaging development within the IBM Systems and Technology Group. He is currently a Research Assistant with the EMC Group, Politecnico di Torino. His research interests include modeling and simulation of interconnect structures, including actual and future chip carriers, multichip and single-chip modules, cards, boards, and connectors. His current research includes modeling and macromodeling of lumped and distributed interconnects for system analysis and design under signal integrity and electromagnetic compatibility constraints.

Flavio G. Canavero (M'90–SM'99–F'07) received the Laurea degree in electronic engineering from the Politecnico di Torino, Turin, Italy, in 1977 and the Ph.D. degree from the Georgia Institute of Technology, Atlanta, in 1986.

He is currently a Professor of circuit theory and electromagnetic compatibility with the Department of Electronics, Politecnico di Torino. His research interests include field coupling to multiwire cables, interconnect and device modeling for signal integrity, and statistical methods in electromagnetic compatibility. He has co-authored more than 150 papers published in international journals and conference proceedings.

Dr. Canavero is the Chair of the Union Radio Scientifique Internationale (URSI) Commission E and a member of the Scientific Steering Committees of several international conferences. He was the Editor-in-Chief of the IEEE TRANSACTIONS ON ELECTROMAGNETIC COMPATIBILITY during 2004–2006.

Ilkka Kelander was born in Vantaa, Finland, in 1975. He received the M.Sc. degree in electrical engineering from Helsinki University of Technology, Espoo, Finland, in 2001.

Since 2000, he has been with Nokia Research Center, Helsinki, Finland. His research interests include electromagnetic design and modeling of electrical packages, modules, and interconnects, and electromagnetic compatibility constraints in mobile devices.

Markku Rouvala received the M.Sc. degree in electrical engineering from Helsinki University of Technology, Espoo, Finland, in 1996.

He was with Nokia Networks from 1996 to 2000 and Stratus Technologies, Maynard, MA, from 2000 to 2002 for hands-on designing for signal integrity on a PCB level for fail-safe computer design. He joined Nokia Mobile Phones, Helsinki, Finland, in 2002, where he managed and participated in successful custom designs for electromechanical miniaturized structures for connectivity. Since 2004, he has been with Nokia Research Center, Helsinki. His current research interests include mobile device connectivity, modeling, and optimization.